

## Bubble propagation in a pipe filled with sand

Damien Gendron,<sup>1,2</sup> Herve Troadec,<sup>1</sup> Knut Jørgen Måløy,<sup>1</sup> and Eirik G. Flekkøy<sup>1</sup>

<sup>1</sup>*Department of Physics, University of Oslo, P.O. Box 1048 Blindern, 0316 Oslo 3, Norway*

<sup>2</sup>*Groupe Matière Condensée et Matériaux, Université de Rennes 1, F-35042 Rennes Cedex, France*

(Received 16 May 2000; revised manuscript received 26 March 2001; published 23 July 2001)

Granular flow with strong hydrodynamic interactions has been studied experimentally. Experiments have been carried out to study the movement of a single bubble in an inclined tube filled with glass beads and air. A maximum bubble velocity was found at an inclined angle  $\theta_m$ . The density variations in the sand were measured by capacitance measurements, and a decompactification zone was observed just above the bubble when the inclination angle  $\theta$  was larger than  $\theta_m$ . The length of the decompactification front increased with increasing inclination angle and disappeared for angles smaller than  $\theta_m$ . Both pressure and visualization experiments were carried out and compared with the density measurements.

DOI: 10.1103/PhysRevE.64.021509

PACS number(s): 83.60.Uv, 81.05.Rm, 83.80.Fg

### I. INTRODUCTION

Transport of granular materials in pipes is of great practical importance and occurs in a large number of industrial processes. Such flows may show localized intermittency effects and density waves which can give rise to permanent clogging of the pipes. The transport of granular materials in a pipe is also of great fundamental interest in the study of density waves [1–5] and related topics like traffic flow [6–8].

When the particles flowing in the tube are small or the interparticle fluid is sufficiently viscous the hydrodynamic interactions between gas and grains are important [9]. Several experiments have been reported where the gas-grain interaction is the dominant flow mechanism. A striking example of this is represented by the intermittent flow in the “ticking” hourglass [10,11] as well as the outflow from various silos [12]. Related experimental studies have been reported on density waves [4,5,13] of granular materials in single tubes where complex wave patterns have been found [4,13].

In this paper we describe an experiment where a bubble is propagating in a tube of sand at different inclination angles  $\theta$ . The granular material will fall faster in an inclined tube [14] than in a vertical tube ( $\theta=90^\circ$ ). We observe a maximum in the bubble speed for an angle  $\theta_m < 90^\circ$ . This effect is similar to and has been compared with [14] the Boycott effect observed for sedimentation in fluids [15]. Boycott observed that blood corpuscles sediment faster in an inclined than in a vertical tube. A qualitative explanation of the Boycott effect is as follows. In sedimentation in a vertical tube, the porous suspension has to pass through the liquid which is a relatively slow process. However, if the tube is tilted, the fluid and particles will start to move in separate “lanes.” The heavier particles will flow down along the lower wall while the fluid moves up along the upper wall, thus producing a large scale convection roll. This particle-fluid separation produces less viscous dissipation and hence a faster motion.

However, the analogy between the bubble in sand and the sedimentation of blood is incomplete. In the experiments we observe that the granular packing *slips* along the tube for

angles larger than  $\theta_m$ . There is no such effect in sedimentation. The maximum velocity of the bubble in the granular column is controlled by the transition between dynamic and static friction of the granular packing above the bubble. This is not the case for sedimentation in liquids where there is no static friction present, and the maximum speed is controlled merely by hydrodynamics.

The focus of the present paper is twofold. First, we study the velocity of the bubble at different inclination angles and packing densities. Second, an experimental technique to measure small density variations in a moving granular packing is introduced and subsequently applied to investigate the origins of the sharp (shock) front that forms in front of the rising bubble. The density variations in the sand were measured by measuring the capacitance across a tube when a bubble passed. For sufficiently steep inclination angles  $\theta$  a clear decompactification zone was observed just above the bubble. We discuss how the latter measurements relate to previous numerical work [16]. As the measurements demonstrate the relatively strong role played by hydrodynamic forces compared to friction, the present work gives support to the assumptions made in the continuum description employed in Ref. [16]. On the other hand, recent theoretical developments [17] together with the present measurements clearly show that the mechanisms governing the bubble motion cannot be fully captured in a coarse grained continuum description. This discussion is detailed in Sec. IV.

### II. EXPERIMENTAL PROCEDURE

In the experiments we used a glass tube which is closed on both sides, with an internal diameter  $D=5$  mm. The tube was mounted on a vertical plate, with a rotation mechanism to tilt the tube (see Fig. 1).

To release a bubble we used two different techniques. In one case the tube, of total length  $l=105$  cm, was partly filled with the granular material with the bubble initially on the top of the tube. The tube was then turned quickly around with the bubble at the bottom to a given inclination angle. This setup was used for velocity and pressure measurements of the bubble. The size of the bubble was determined by the amount of grains initially filled in the tube.

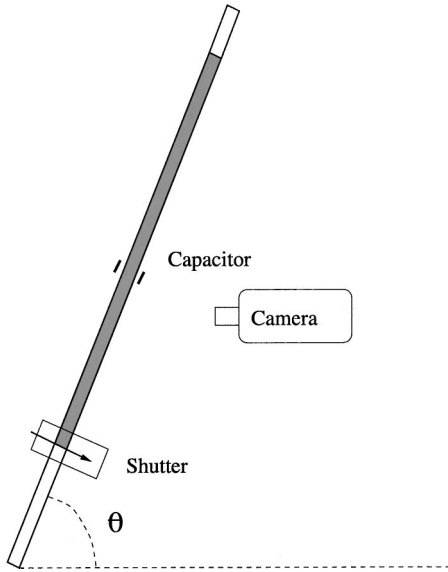


FIG. 1. The experimental setup with capacitance measurements and ultrafast video recording.

In the second case, the tube is divided into two pieces of length 15 cm and 100 cm. The upper 100 cm of the tube was filled with granular material and the lower 15 cm was filled with air. A mechanical shutter is placed between the upper and the lower tube. The shutter consists of a 0.5 mm thick aluminum plate with a hole of diameter 5 mm. The plate was moved so as to place the hole in the center of the tube and release the bubble. The shutter mechanism was externally sealed to prevent air leakage from the granular packing. Both the upper and the lower parts were initially kept at atmospheric pressure. The density variations in the sand were measured by means of a capacitor mounted at a height 25 cm from the shutter. The capacitor consists of two plates of length 1 cm located on each side of the glass tube. The capacitor was screened by a Faraday cage to prevent external noise. An increase in the amount of sand between the capacitor plates will increase the capacitance. The capacitance was calibrated by performing experiments with tubes of sand with different densities. A low density of sand were obtained in the calibration experiments by fluidizing the sand by blowing air through the packing. Within the available solid fractions between 0.50 and 0.60 obtained in the calibration experiments, we found the solid fraction to vary linearly as  $c - c_c = -(3.1/pF)(C - C_c)$ . This relation also gives the right value for the capacitance of the empty tube. Here  $C_c$  is the capacitance of the compactified powder,  $C$  is the measured capacitance, and  $c$  and  $c_c$  are the corresponding solid fractions.

The “sand” used in the experiments consists of spherical glass beads of diameter  $d = 65 \mu\text{m}$  and glass density  $\rho_g = 2.47 \text{ g cm}^{-3}$ . The air humidity was kept within  $(27 \pm 3)\%$  during the tube filling procedure. The experiments were performed with two different solid fractions  $c = 1 - \phi$ . Here  $\phi$  is the porosity of the sand. The lowest solid fraction  $c_l = 0.56$  and density  $\rho_l = 1.38 \text{ g cm}^{-3}$  was obtained by gently filling the vertical tube with glass beads from the top. A higher solid fraction  $c_c = 0.60$  and  $\rho_c = 1.48 \text{ g cm}^{-3}$  was ob-

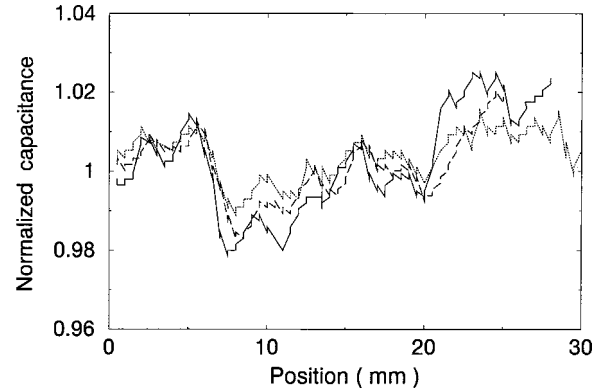


FIG. 2. Normalized capacitance variation as function of tube position for the high solid fraction (solid line), low solid fraction (dashed line), and empty tube (dotted line).

tained by repeating the same procedure as above, followed by careful tapping on the tube wall until the packing reached the desired height. In order to check that this procedure gives a homogeneous solid fraction along the tube, the capacitance was measured at different positions.

Figure 2 shows the capacitance (divided by the average capacitance) along the tube plotted as a function of the capacitor position for the uncompacted sample, the compactified sample, and the empty tube. We note that there are strong correlations between these measurements and the capacitance variations of the same but empty tube. Hence the main part of the fluctuations in the capacitance is due to thickness fluctuations of the glass walls and not due to fluctuations in the solid fraction. Only a small variation in the capacitance (less than  $\pm 0.5\%$ ) is due to density fluctuations of the powder. This corresponds to less than  $\pm 1.5\%$  fluctuation in the solid fraction.

To study the dynamics and the local density fluctuations of the bubble we used an ultrafast video camera (Kodak Motion Corder SR-1000). Pictures were taken at a speed of up to 1000 pictures per second with a shutter time of  $10^{-4} \text{ s}$ .

To measure the pressure in the tube we used a pressure sensor based on the deviation of a laser beam due to reflection from a bending glass plate. We designed this sensor for the measurements on the hourglass [11]. The pressure sensor was connected at a distance  $l/2$  from the bottom of the tube. The connection was made by a 0.5 mm hole, connected by a tube to the sensor. The sensor did not cause any visible perturbation of the bubble.

### III. EXPERIMENTAL RESULTS

#### A. Bubble velocity

The average speed of the bubble was measured for two different solid fractions at different inclination angles  $\theta$  (see Fig. 3). Movement of the bubble starts at an angle close to  $30^\circ$ . The propagation velocity of the bubble increases with increasing angle until it reaches a maximum at  $\theta_m$ , which is significantly lower than  $90^\circ$ . An important visual observation in these experiments was that the top level of the sand did not move at angles lower than  $\theta_m$ . On the other hand, when

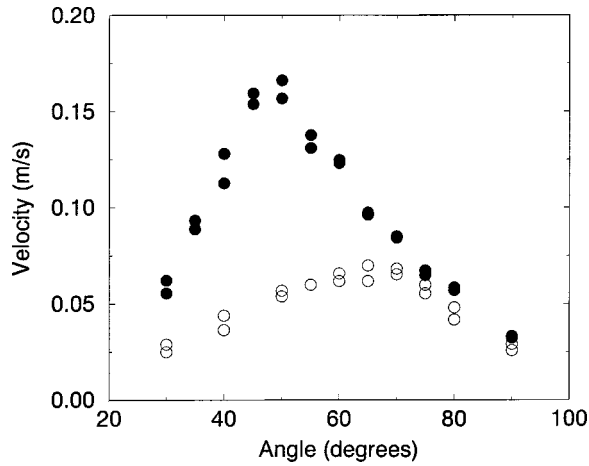


FIG. 3. The dependence of the bubble velocity on the inclination angle for two different solid fractions  $c=0.55$  (filled symbols) and  $c=0.60$  (open symbols). The particle size is  $d=65 \mu\text{m}$ .

the angle became larger than  $\theta_m$ , movement of the top level was observed. This shows that the sand slips along the wall for angles larger than  $\theta_m$ .

Figure 3 shows that the bubble velocity is higher in the tube with the lower solid fraction. This is because the friction forces have increased with the increased density of the sand.

When the tube is close to vertical, the speed of the bubble is insensitive to the initial solid fraction. This insensitivity in the speed may indicate a low density zone above the bubble that is insensitive to the initial solid fraction. This low density zone was observed both in the capacitance measurements and directly by fast video recordings, as described below.

### B. Fast photography visualization of the bubble

Visualization experiments have been performed with a fast charge-coupled device camera to study local dynamics and density fluctuations inside the bubble. Figure 4 shows detailed pictures of the bubble at an inclination angle  $\theta=90^\circ$ . It is clear from these pictures that the density of the sand inside the bubble is not homogeneously distributed but has strong local fluctuations. We also observe that the particles are not released homogeneously from the top of the bubble, but rather in “bursts” of different sizes.

Figure 5 shows pictures of the bubble at an inclination angle  $\theta=70^\circ$ . A very different behavior is observed in this case. The sand inside the bubble is sliding along the sidewall and convection is observed at the bottom of the bubble where particles move upward again. The convection at the bottom of the bubble has been discussed in a recent paper [14] where the authors emphasize the very efficient mixing obtained by the convection process. On closer inspection of the top of the bubble we observe a ripple propagating downward along the surface of the flowing grains. This ripple, which is most easily observed in motion, is shown in Fig. 6.

The fast camera was further used to observe the particle movement above the bubble. For  $\theta=90^\circ$ , a stick-slip behavior was observed at heights more than 10 cm above the bubble. The particles stopped at regular intervals of about 0.4

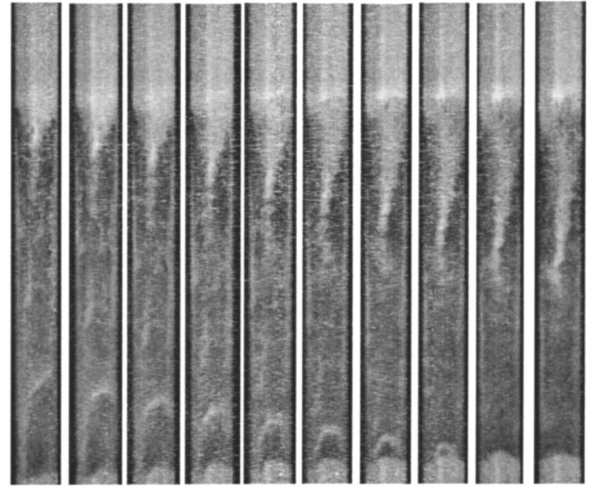


FIG. 4. Pictures of the bubble at an inclination angle  $\theta=90^\circ$ . The time is increasing from left to right with 0.004 s between each picture. Strong inhomogeneities are seen inside the bubble. The size of the picture is given by the internal diameter of the tube, which is 5 mm.

s. However, we also observed that at a distance less than approximately 7 cm above the bubble the particles did not come to a complete stop. Thus no stick-slip motion was observed at this location above the bubble. This observation is supported by the capacitance measurements of the low density zone described below.

### C. Capacitance measurements

Capacitance measurements were performed to investigate density variations in the granular packing. A bubble of 15 cm was released and the capacitance was measured as a function of time by a capacitor located 25 cm above the mechanical shutter. When the inclination angle was larger than  $\theta_m$  a decompactification zone was observed above the bubble. Although the existence of this zone was indicated by the absence of stick-slip motion seen in the video recordings, the



FIG. 5. Pictures of the bubble at an inclination angle  $\theta=70^\circ$ . The time is increasing from left to right with 0.008 s between each picture. Convection is seen on the bottom of the bubble. The size of the picture is given by the internal diameter of the tube, which is 5 mm.

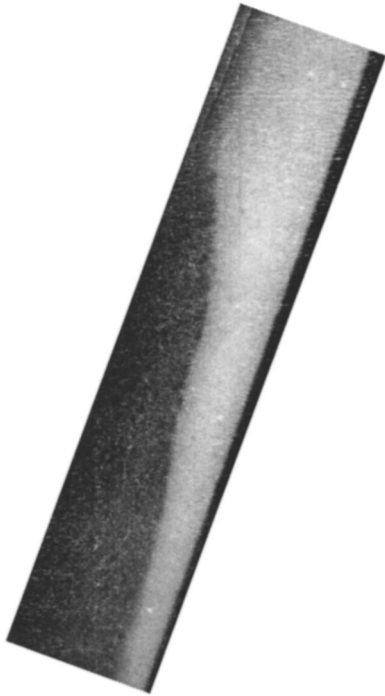


FIG. 6. Picture of the top of the bubble for an inclination angle  $\theta=70^\circ$ . A ripple is observed propagating downward. The size of the picture is given by the internal diameter of the tube, which is 5 mm.

only direct evidence of it comes from the capacitance measurements. Visually the decompactification zone cannot be directly observed.

For  $\theta < \theta_m$  no decompactification zone was observed. In Fig. 7 and Fig. 8, the dependence of the solid fraction as a function of time is shown for the inclination angles  $\theta=80^\circ$  and  $\theta=90^\circ$ . The solid fraction  $c$  decreases from the value  $c=0.60$  to a plateau of about  $c=0.58$  just in front of the bubble. A sharp shock front with a decrease in the solid fraction from  $c=0.58$  to about  $c=0.08$  identifies the top of the bubble. The bottom of the bubble is seen as a sharp increase in the solid fraction from 0.08 to 0.56. It is important to note that the solid fraction is calculated under the assumption that the sand is homogeneously distributed in the

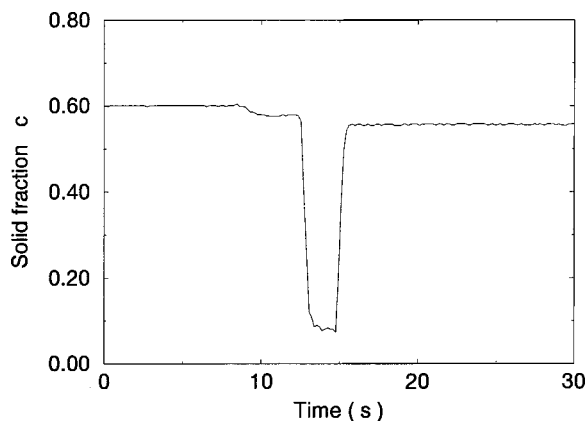


FIG. 7. The solid fraction  $c$  as a function of time at an inclination angle  $\theta=80^\circ$ . The bead size  $d=65 \mu\text{m}$ .

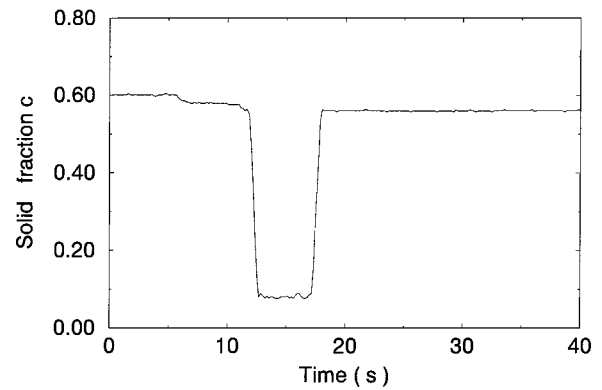


FIG. 8. The solid fraction  $c$  as a function of time at an inclination angle  $\theta=90^\circ$ . The bead size  $d=65 \mu\text{m}$ .

tube. However, from the visualization experiments we know that this is not the case and that there are local density fluctuations inside the bubble. These measurements therefore just give an estimate of the solid fraction of sand averaged over the capacitor size.

In Fig. 9, the length of the plateau of the decompactification zone is shown as a function of the inclination angle. The low density zone is observable for angles larger than  $\theta_m$ , and increases roughly linearly with increasing inclination angle.

#### D. Pressure measurements

From visual observations the top layer was observed to move at angles larger than  $\theta_m$ . A movement of the packing above the bubble will compress the gas. A pressure increase is therefore expected inside the bubble with a pressure gradient between the bubble and the top level of the sand.

To check this in more detail, pressure measurements were performed in the middle of the tube as a function of time (see Fig. 10). To determine the location of the bubble, the laser beam used in the pressure measurements was blocked manually when the top and the bottom of the bubble passed the sensor and when the bubble reached the top of the granular

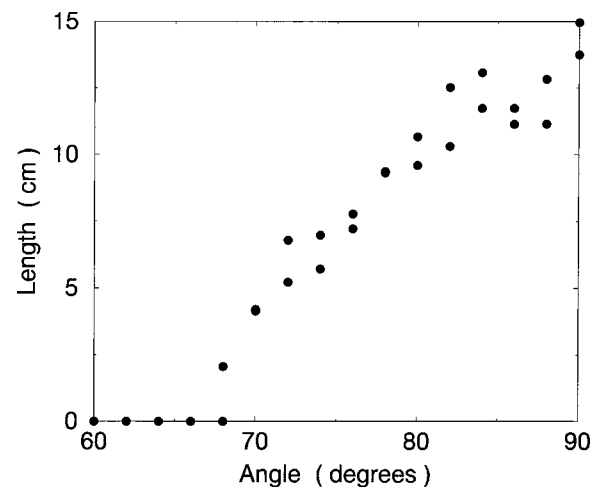


FIG. 9. The dependence of the length of the decompactification zone on the inclination angle  $\theta$  for a particle of diameter  $d=65 \mu\text{m}$ .

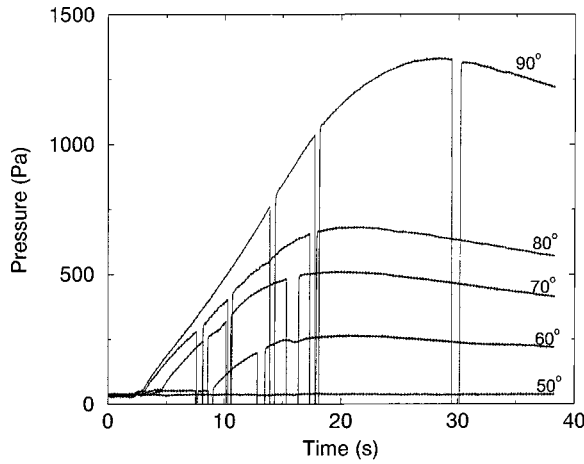


FIG. 10. The dependency of the pressure on time for different inclination angles during propagation of a bubble. The experiment is performed at low solid fraction  $c_l=0.56$  with  $65 \mu\text{m}$  beads.

packing. Thus in each graph the three dips correspond to the passing of the top and the bottom of the bubble and when the top of the bubble reaches the surface. For angles lower than  $\theta_m$  no pressure effects were observed. However, for angles larger than  $\theta_m$  a significant increase in the pressure was observed until the bubble reached the top of the packing. For larger times the pressure decreased again due to flow of gas out of the packing followed by a compactification of the granular material.

Figure 11 and Fig. 12 show the dependence of the pressure at the top and the bottom of the bubble on the inclination angle  $\theta$ . The same figures also show the propagation velocity together with the pressure in the packing just when the bubble reaches the top. In all cases the pressure in the packing increases with increasing angle when  $\theta > \theta_m$ .

IV. DISCUSSION

There is a qualitative difference between the bubble propagation when the angle is smaller or larger than  $\theta_m$ . For

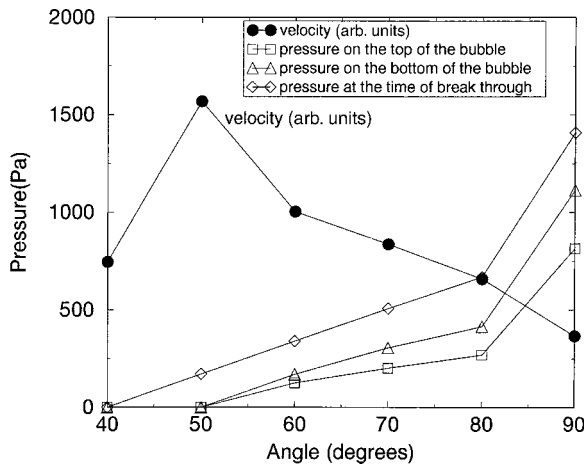


FIG. 11. The velocity in arbitrary units, the pressure at the top of the bubble, the pressure at the bottom of the bubble, and the pressure when the bubble reaches the top of the packing. The data are shown for different angles with  $65 \mu\text{m}$  beads and a low solid fraction  $c_l=0.56$ .

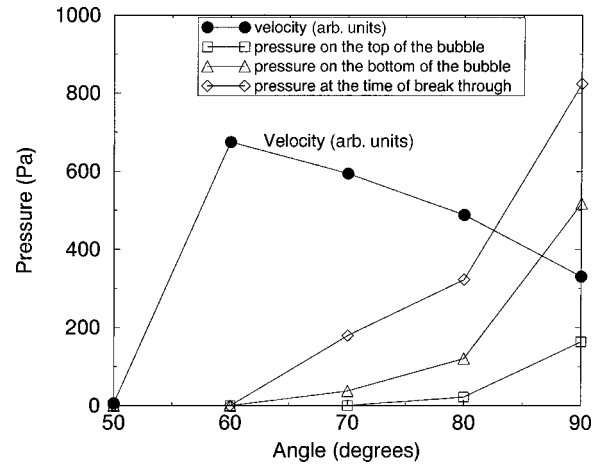


FIG. 12. The velocity in arbitrary units, the pressure at the top of the bubble, the pressure at the bottom of the bubble, and the pressure when the bubble reaches the top of the packing. The data are shown for different angles with  $65 \mu\text{m}$  beads and high solid fraction  $c_c=0.60$ .

angles lower than  $\theta_m$  static friction from the walls prevents granular motion above the bubble as well as compression of the bubble. In the regime where  $\theta < \theta_m$  the velocity of the bubble is increasing with increasing angle. No motion of the top level indicating slip is observed. The density is constant above the bubble with a sharp density change at the top of the bubble.

In the regime where  $\theta > \theta_m$ , the velocity is decreasing with increasing  $\theta$ . Motion of the top layer occurs, indicating slip of the packing and dynamic friction. The slip gives a compactification of the air in the bubble with a pressure increase which sets up a pressure gradient across the packing. This pressure gradient increases the viscous drag acting on the particles.

One of the fundamental problems in the description of granular materials is to locate and define the appropriate boundary conditions between the regions where the granular medium behaves more like a solid (with rigid response to shearing forces) and where it behaves more like a liquid (which may deform continuously) [4,16,18]. Due to the local expansion, or dilatancy [19], that must take place in order for shear motion to occur in a granular medium these boundaries may be quite sharp. Many types of granular flow that are not strongly excited [10,20] will be governed by the presence of both liquid- and solidlike behavior. The fact that the granular packing slips for angles larger than  $\theta_m$  demonstrates that a “solid-liquid” interface is present and makes this problem qualitatively different from the Boycott effect observed in sedimentation in fluids. The maximum velocity of the bubble is controlled by the transition between dynamic and static friction of the granular packing above the bubble. This is not the case for sedimentation in liquids where there is no static friction, and the maximum speed is controlled by hydrodynamics.

The existence of the decompactification zone and the fact that there is no stick-slip motion right above the bubble are both indications that the shock front on the top of the bubble is caused mainly by hydrodynamic effects. A recent theoret-

ical consideration assuming a constant granular density down to the top of the bubble indicated that when averaged over local volume elements the hydrodynamic forces acting upward on the grains will always exceed the downward acting forces of gravity [17], thus suppressing entirely the propagation of the bubble. If this is the situation the bubble will not move upward, but the top interface will fall downward due to gas leakage through the packing. However, the experimental observation presented in this paper clearly shows that the particles fall through the bubble and that the density just above the bubble is significantly lower than farther up in the granular packing. Since the experiments show bubbles that propagate with a sharp front, this implies that local details in the density variations are crucial for the bubble motion. On the other hand, while the quoted theoretical findings show that the correct mechanisms for the release of particles on top of the bubble cannot really be captured in a continuum model, the effect of these mechanisms may still be handled in such a context. This is the case in a recent paper [16] where the bubble-sand interface is blurred by the addition of a diffusive mechanism. A qualitative and a reasonable quantitative agreement were found between the simulations and corresponding experiments.

The present experimental findings of a reduction in the density above the bubble strongly indicate a corresponding

reduction in the friction. If the friction is negligible in the low density zone, this may justify the approximation of neglecting the friction in our previous simulations. However, the wall friction above the low density zone will cause the bubble to decrease in size more slowly than if the wall friction is zero. This effect was also seen in the comparison between the experiments and the simulation in Ref. [16].

The gas pressure gradient in the packing will depend on the friction from the tube walls. The stick-slip motion in the upper part of the packing will thus couple to the gas pressure in the bubble, which in turn governs the release of particles in the top of the bubble. The stick-slip motion may thus produce via the pressure an inhomogeneous and intermittent release of particles in the top front, as is observed in the fast video recordings. The observed stick-slip motion in the upper part of the packing was not observable in the pressure measurements. This may be due to limited resolution of the pressure sensor.

#### ACKNOWLEDGMENTS

The authors thank Daniel Bideau and Thierry Le Penec for valuable comments. We would like to thank CNRS and NFR for support of an exchange program between France and Norway.

- 
- [1] H.J. Herrmann, in *Mobile Particulate Systems*, edited by E. Guazzelli and L. Oger (Kluwer Academic Publishers, London, 1995), p. 281.
  - [2] S.B. Savage, *J. Fluid Mech.* **244**, 109 (1992).
  - [3] C.K.K. Lun and S.B. Savage, *J. Fluid Mech.* **140**, 223 (1984).
  - [4] T. Raafat, J.P. Hulin, and H.J. Herrmann, *Phys. Rev. E* **53**, 4345 (1996).
  - [5] A. Nakahara and T. Isoda, *Phys. Rev. E* **55**, 4264 (1997).
  - [6] M.J. Lighthill and G.B. Witham, *Proc. R. Soc. London, Ser. A* **229**, 317 (1955).
  - [7] T. Musha and H. Higuichi, *Jpn. J. Appl. Phys.* **15**, 1271 (1976).
  - [8] K. Nagel and M. Schreckenberg, *J. Phys. I* **2**, 2221 (1992).
  - [9] S.M. Namara, E.G. Flekkøy, and K.J. Måløy, *Phys. Rev. E* **61**, 4054 (2000).
  - [10] X.L. Wu *et al.*, *Phys. Rev. Lett.* **71**, 1363 (1993).
  - [11] T.L. Pennec *et al.*, *Phys. Rev. E* **53**, 2257 (1996).
  - [12] T.L. Pennec *et al.*, *Phys. Fluids* **10**, 3072 (1998).
  - [13] J.L. Aider, N. Sommier, T. Raafat, and J.P. Hulin, *Phys. Rev. E* **59**, 778 (1999).
  - [14] J. Duran and T. Mazozi, *Phys. Rev. E* **60**, 6199 (1999).
  - [15] A.E. Boycott, *Nature (London)* **104**, 532 (1920).
  - [16] E.G. Flekkøy and K.J. Måløy, *Phys. Rev. E* **57**, 6962 (1998).
  - [17] E.G. Flekkøy and K. J. Måløy (unpublished).
  - [18] K. Nagel and H.J. Herrmann, *Physica A* **199**, 254 (1993).
  - [19] O. Reynolds, *Philos. Mag.* **20**, 469 (1885).
  - [20] G.W. Baxter, R.P. Behringer, T. Fagert, and G.A. Johnson, *Phys. Rev. Lett.* **62**, 2825 (1989).